Thallous Ion Movements through Gramicidin Channels Incorporated in Lipid Monolayers Supported by Mercury

Lucia Becucci, Maria Rosa Moncelli, and Rolando Guidelli
Department of Chemistry, Florence University, 50121 Florence, Italy

ABSTRACT The potential independent limiting flux of hydrated Tl^+ ions through gramicidin (GR) channels incorporated in phospholipid monolayers self assembled on a hanging mercury-drop electrode is shown to be controlled both by diffusion and by a dehydration step. Conversely, the potential independent limiting flux of dehydrated Tl^+ ions stemming from Tl amalgam eletrooxidation is exclusively controlled by diffusion of thallium atoms within the amalgam. Modulating the charge on the polar heads of dioleoylphosphatidylserine (DOPS) by changing pH affects the limiting flux of hydrated Tl^+ ions to a notable extent, primarily by electrostatic interactions. The dipole potential of DOPS and dioleoylphosphatidylcholine (DOPC), positive toward the hydrocarbon tails, does not hinder the translocation step of Tl^+ ions to such an extent as to make it rate limiting. Consequently, incorporation in the lipid monolayer of phloretin, which decreases such a positive dipole potential, does not affect the kinetics of Tl^+ flux through GR channels. In contrast, the increase in the positive dipole potential produced by the incorporation of ketocholestanol causes the translocation step to contribute to the rate of the overall process. A model providing a quantitative interpretation of the kinetics of diffusion, dehydration–hydration, translocation, and charge transfer of the Tl^+/Tl^0(Hg) couple through GC channels incorporated in mercury-supported phospholipid monolayers is provided. A cut-off disk model yielding the profile of the local electrostatic potential created by an array of oriented dipoles located in the lipid monolayer along the axis of a cylindrical ion channel is developed.

INTRODUCTION

Gramicidin (GR) is a linear, hydrophobic pentadecapeptide that forms ionic channels in artificial and natural membranes (Andersen and Koeppe, 1992; Koeppe and Andersen, 1996; Hladky and Haydon, 1984; Killian, 1992; Busath, 1993). It is generally accepted that membrane-spanning GR channels are dimers formed by transmembrane association of two single-stranded right-handed helical monomers, which are joined at their formyl NH-termini. The dipole potential was found to affect the ionic conductance of the GR channel, albeit to a much lower extent than in the case of carrier-mediated cation transport (Bamberg et al., 1976; Providence et al., 1995). This behavior agrees with theoretical conclusions by Jordan (1983), who predicts substantial shielding of the dipole potential within the ion channel (see also Malkov and Sokolov, 1996). The small, but detectable, effect of the dipole potential on GR conductance may also be ascribed to an indirect cause, namely an appreciable change in the GR channel lifetime. Thus, GR lifetime differs considerably for membranes formed with ether or ester lipids (Providence et al., 1995; Seoh and Busath, 1995). Phloretin, known to decrease the dipole potential (Andersen et al., 1976; Melnik et al., 1977; Pohl et al., 1997), decelerates the flash-induced decay of GR-mediated ionic conductance, whereas 6-ketocholestanol (KC), known to increase the dipole potential (Franklin and Cafiso, 1993; Gross et al., 1994), accelerates such a decay (Rokitskaya et al., 1997). Moreover, single-channel data show that phloretin causes an increase in the lifetime of GR channels (Rokitskaya et al., 1997).

The length of a GR monomer matches that of a lipid monolayer, just like that of a GR dimer matches that of a lipid bilayer. The monomer of GR incorporated in a mercury-supported phospholipid monolayer was reported by Nelson (1991) to act as an ion channel toward Tl^+ ion, thus allowing its penetration across the monolayer and its electroreduction to Tl amalgam. From a cyclic voltammetric and a chronoamperometric investigation of Tl^+ ion electroreduction through GR channels, Nelson proposed a chemical electrochemical mechanism, in which the rate-determining step is a preceding homogeneous chemical step associated with Tl^+ entry into the channel prior to Tl^+ electroreduction. This electrode process at a mercury-supported phospholipid monolayer incorporating GR was used by Nelson as a model system to probe the effect of lipid charge (Nelson, 1997), solution composition and incorporation of biologically active compounds (Nelson, 1996) on ion channel transport. Rueda et al. (1999) investigated Tl^+ electroreduction across GR-modified dioleoylphosphatidylcholine (DOPC) monolayers on mercury by electrochemical impedance spectroscopy. Nelson and Bizzotto (1999), in examining this system by chronoamperometry, regarded the homogeneous chemical step preceding charge transfer as related to complex formation of Tl^+ ion within the ion channel.

The use of self-assembled phospholipid monolayers supported by mercury dates back to the pioneering work of Miller and Bach (1969), who described the self-assembly of phospholipid monolayers on a dropping mercury electrode.

Submitted May 16, 2001 and accepted October 25, 2001.

Address reprint requests to Rolando Guidelli, Dept. of Chemistry, Florence University, Polo Scientifico, Via della Lastruccia 3, 50019 Sesto Fiorentino, (Firenze), Italy. Tel.: 39-055-2757540; Fax: 39-055-244102; E-mail: guidelli@unifi.it.

0006-3495/02/02/852/13 $2.00

From then on, phospholipid self-assembled monolayers on mercury electrodes have been extensively investigated for their applications as models of biological membranes. Molecules of biological importance (Herrero et al., 1997, 1998, 2000; Moncelli et al., 1996, 1998a; Nelson, 1992), lipophilic ions (Moncelli et al., 1995), peptides and proteins (Lecompte and Miller, 1980; Lecompte et al., 1998; Miller et al., 1978) have been incorporated in Hg-supported phospholipid monolayers with the aim of investigating their behavior in an environment mimicking that of biological membranes. These monolayers have the hydrocarbon tails directed toward the hydrophobic mercury surface and the polar heads directed toward the solution (Nelson and Benton, 1986). They have a high mechanical stability, a high resistance to electric fields, and a notable reproducibility. Over the potential range from -0.2 to -0.8 V versus the saturated calomel electrode (SCE) they behave like a half-membrane. Thus, they are impermeable to inorganic ions, and their differential capacity is $\sim 1.7\ \mu F\ cm^{-2}$, namely twice that of black lipid membranes (BLMs). There is clear evidence that the interface between an aqueous phase and a lipid monolayer is equivalent to that between the same aqueous phase and a lipid bilayer. Thus, the intrinsic pK_a values for DOPC and dioleoylphosphatidylamine obtained from differential capacity measurements in mercury-supported monolayers agree with those obtained in vesicles, Langmuir–Blodgett monolayers and BLMs (Moncelli et al., 1994). The apparently anomalous features of the pK_a values for dioleoylphosphatidylserine (DOPS) in mercury-supported monolayers (Moncelli et al., 1994, 1998b) have been recently confirmed in BLMs by Ermakov et al. (2001). The adsorption isotherms of tetraphenylphosphonium and tetraphenylborate in mercury-supported DOPC and DOPS monolayers, as determined from the charge flowing along the external circuit as a consequence of the translocation of these lipophilic ions across the monolayer (Moncelli et al., 1995), agree with those determined in BLMs. The surface dipole potentials of DOPC and DOPS monolayers determined from the charge following the progressive expansion of a mercury drop supporting these monolayers (Becucci et al., 2000) are in fairly good agreement with those determined in BLMs. For all the above reasons, as long as interactions with foreign molecules do not extend beyond the hydrocarbon tail region facing the mercury surface, no appreciable differences between mercury-supported monolayers and BLMs are expected.

The investigation of Tl^+ electroreduction in GR-modified self-assembled lipid monolayers supported by mercury exhibits some advantageous features. Thus, the high sensitivity of this system to Tl^+ flux across GR channels allows measurements at Tl^+ bulk concentrations as low as 10^{-5} M. Because the equilibrium binding constant of Tl^+ ion with GR is $\sim 500\ M^{-1}$ (Hinton et al., 1986, 1988), at these low Tl^+ concentrations, the fraction of GR channels occupied by Tl^+ ions is negligible. Moreover, the electroreduction rate of Tl^+ ions in direct contact with the mercury surface is so high (Agarwal, 1974), that the probability of dual occupancy of GR monomers by Tl^+ ions is extremely low. The kinetics of Tl^+ translocation across GR channels can also be investigated starting from the dehydrated Tl^+ ion that results from Tl amalgam electrooxidation, providing further pieces of information. Finally, the effect of lipophilic neutral species known to alter the dipole potential of membranes, such as the steroids KC and phloretin, upon the kinetics of ion movement through monomeric GR channels permits one to exclude the contribution from the dissociation kinetics of GR dimers. The present paper aims at exploiting the above advantageous features. A model providing a quantitative interpretation of the kinetics of diffusion, dehydration–hydration, translocation, and charge transfer of the Tl^+/Tl^0(Hg) couple through GR channels incorporated in mercury-supported phospholipid monolayers will be provided. A cut-off disk model yielding the profile of the local electrostatic potential created by an array of oriented dipoles located in the lipid monolayer along the axis of a cylindrical ion channel will be developed and applied to the retarding effect of KC on Tl^+ flux through GR channels.

MATERIALS AND METHODS

All inorganic salts were purchased from Merck (Milano, Italy). DOPC from Lipid Products (South Nutfield, Surrey, U.K.), DOPS from Avanti Polar Lipids (Birmingham, AL), phloretin, tetramethylammonium, and tetraethylammonium chloride from Fluka (Milano, Italy), gramicidin D and KC from Sigma (Milano, Italy), were used without further purification. The water used was obtained from light mineral water by distilling it once, and by then distilling the resulting water from alkaline permanganate, discarding the heads. Reagent-grade KCl was baked at 500°C before use to remove any organic impurities. All measurements were carried out in deaerated aqueous solutions of 0.1 M KCl at 25 ± 0.1°C. Potassium ion can bind to the mouth of the GR channel but it cannot permeate it, because it is not electroreduced with amalgam formation over the potential range investigated. Its effect on Tl^+ flux is expected to be negligible. In fact, the use of 0.1 M tetramethylammonium or tetraethylammonium in place of K^+ yields practically identical results, even though these organic cations have lower binding constants with GR (Hinton et al., 1988). The pH was controlled with 1×10^{-3} M phosphate buffer, varying the ratio of its differently protonated forms through the addition of suitable amounts of HCl or NaOH.

Monolayers of DOPC and DOPS were self assembled on mercury as described earlier (Moncelli et al., 1994, 1996; Nelson and Benton, 1986). The home-made hanging mercury-drop electrode (HMDE) and the cell used in the measurements are described elsewhere (Moncelli et al., 1994; Moncelli and Becucci, 1997). Differential capacity measurements were carried out using a Metrohm Polarecord E506 (Herisau, Switzerland). The AC signal had a 10-mV amplitude and a 75-Hz frequency. The system was calibrated using a precision capacitor. All potentials were measured versus a saturated calomel electrode (SCE) and are referred to this electrode. Tl^+ electroreduction and Tl^0(Hg) electrooxidation across a GR-modified lipid monolayer, self assembled on mercury and on Tl amalgam, respectively, were investigated by a chronocoulometric procedure described elsewhere (Moncelli et al., 1995). To this end, a wholly computerized apparatus (Foresti et al., 1980) was used. The microprocessor used to control all the operations was a Model NOVA 4X from Data General (Westboro, MA),

and an Amel Model 551 (Milano, Italy) potentiostat with a rise time of 0.5 μs was used for the potentiostatic control of the three-electrode system. The detailed scheme of the home-made electronic current integrator working under microprocessor control is described in Carlà et al. (1988).

Each chronocoulomogram for Tl^+ electroreduction consisted of a series of consecutive potential jumps of progressively increasing height from a fixed initial value E_i of -0.250 V to different final values E ranging from -0.250 to -0.750 V, and was recorded on a single lipid-coated mercury drop. The charge $Q(t, E)$ following each potential jump $E_i \rightarrow E$ was recorded versus the time t elapsed from the instant of the jump for 100 ms, after which the potential was stepped back to E_i, where it remained for one s. During this period Tl^0(Hg) was completely reconverted to Tl^+ ion. Thus, an increase in the rest time at E_i beyond 1 s left the charge $Q(t, E)$ practically unaltered. The chronocoulomograms for Tl^0(Hg) electrooxidation on a lipid-coated Tl amalgam electrode were recorded by an analogous procedure, stepping from a fixed initial potential of -0.750 V to progressively more positive potentials E. Curves of the current i(100 ms, E) versus E were obtained by sampling the charge ΔQ flowing between 98 and 102 ms from the instant of each potential step $E_i \rightarrow E$ and dividing it by $\Delta t =$ 4 ms. Before using a newly formed lipid-coated mercury drop for chronocoulometric measurements, the good quality of the lipid monolayer was checked by recording a curve of the differential capacity C versus E in aqueous 0.1 M KCl. Each series of chronocoulometric measurements at different pH values was carried out on a single lipid-coated mercury drop.

Hanging Tl amalgam-drop electrodes containing 4×10^{-4} M Tl^0(Hg) were prepared by applying a potential of -0.750 V to a bare HMDE immersed in a deaerated aqueous solution of 0.1 M KCl containing 4×10^{-4} M Tl^+ for a time long enough to obtain a plateau for Tl^0(Hg) electrooxidation of the same height as that for Tl^+ electroreduction. The Tl^+ ion was then gradually removed from the cell by substituting progressive volumes of the Tl^+ solution with equal volumes of aqueous 0.1 M KCl alone, to keep the Tl amalgam drop constantly immersed in the deaerated solution. The Tl amalgam drop was then coated with a lipid monolayer incorporating GR by the same procedure adopted for a mercury drop. Incorporation of GR in a lipid-coated mercury or Tl amalgam drop immersed in the solution was carried out by dissolving GR in the solution and by stirring gently for a time long enough to attain adsorption equilibrium.

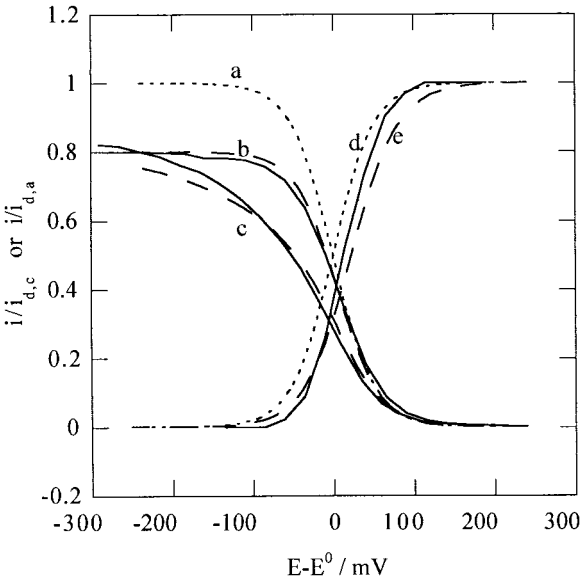

FIGURE 1 Plots of the ratio of the current i for 4×10^{-4} M Tl^+ electroreduction or 4×10^{-4} M Tl^0(Hg) electrooxidation to the corresponding diffusion limiting value, $i_{d,c}$ or $i_{d,a}$, against $(E - E^0)$, where E^0 is the formal potential of the Tl^+/Tl^0(Hg) couple. All curves were obtained from aqueous 0.1 M KCl. Tl^+ reduction waves on (*a*) bare mercury, on (*b*) DOPC-coated mercury in the presence of 1.5×10^{-7} M GR, and (*c*) on (DOPC + 23 mol% KC)-coated mercury in the presence of 1.5×10^{-7} M GR. Tl^0(Hg) oxidation waves on (*d*) bare Tl amalgam and on (*e*) (DOPC + 23 mol% KC)-coated amalgam in the presence of 1.5×10^{-7} M GR. Dotted and solid curves are experimental plots, dashed curves were calculated as described in the text.

RESULTS

On a bare mercury electrode, Tl^+ ion is electroreduced to Tl^0(Hg), giving rise to a sigmoidal curve of the current i against the applied potential E (*dotted curve a* in Fig. 1). Its rising section exhibits a Nernstian behavior, and its plateau is exclusively controlled by diffusion. A Nernstian behavior with diffusion control is also exhibited by the i versus E curve for Tl^0(Hg) electrooxidation on a bare Tl amalgam electrode (*dotted curve d* in Fig. 1). The common half-wave potential of the two curves provides the formal potential for the Tl^+/Tl^0(Hg) couple, which amounts to -0.463 V. If the electrode is coated with a phospholipid monolayer, neither Tl^+ nor Tl^0(Hg) can permeate the film, and hence no reduction or oxidation current is observed. If GR is incorporated in the lipid monolayer from a 1.5×10^{-7} M solution of this ion channel-forming peptide, the sigmoidal i versus E curve for Tl^+ electroreduction reappears, as shown by the solid curve b in Fig. 1. However, its plateau is now lower, denoting mixed control by diffusion and by some potential-independent step (Nelson and Bizzotto, 1999). This is also confirmed by the shape of the potentiostatic curves of the charge $Q(t, E)$ versus time t in Fig. 2, recorded at potentials along the rising portion and the plateau of the i versus E curve b in Fig. 1: none of these $Q(t, E)$ versus t curves exhibits the typical linear increase of charge with the square root of the electrolysis time t, which characterizes pure linear diffusion control according to the Cottrell equation. Occasionally, the current shows a slight decrease at potentials negative of -0.60 V. At ~ -0.80 V, it increases rapidly, attaining its diffusion limiting value, due to the increased permeability of the phospholipid monolayer (Nelson and Bizzotto, 1999). An increase in the GR bulk concentration from 1×10^{-9} to 1.5×10^{-7} M causes the plateau of the Tl^+ wave to increase less than linearly, attaining a saturation value. The following results were obtained with a GR bulk concentration of 1.5×10^{-7} M. This relatively high value allows GR incorporation in the lipid film to attain its equilibrium value rapidly, by mild stirring of the solution for 10 min. At constant GR bulk concentration, the height of the Tl^+ wave increases proportionally to the bulk Tl^+ concentration over the range from 5×10^{-5} to 5×10^{-3} M. A 4×10^{-4}-M Tl^+ concentration was normally adopted. A peculiar feature of the solid curve b in Fig. 1 for Tl^+ electroreduction is represented by its half-wave potential being more positive than the formal potential of the Tl^+/Tl^0(Hg) couple by $\sim$6 mV. As distinct from the i versus E curve for Tl^+ electroreduction, that for

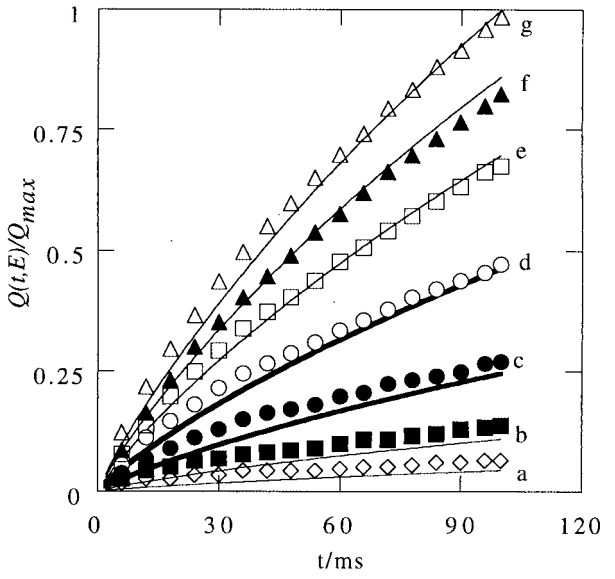

FIGURE 2 Potentiostatic curves of the charge $Q(t, E)$ for 4×10^{-4} M Tl^+ electroreduction on DOPC-coated mercury from aqueous 0.1 M KCl containing 1.5×10^{-7} M GR against the electrolysis time t. Charges are normalized to their maximum value. Experimental values are denoted by markers, solid curves were calculated. Applied potential E: (*a*) −0.375, (*b*) −0.400, (*c*) −0.425, (*d*) −0.450, (*e*) −0.475, (*f*) −0.500, and (*g*) −0.600 V versus the SCE.

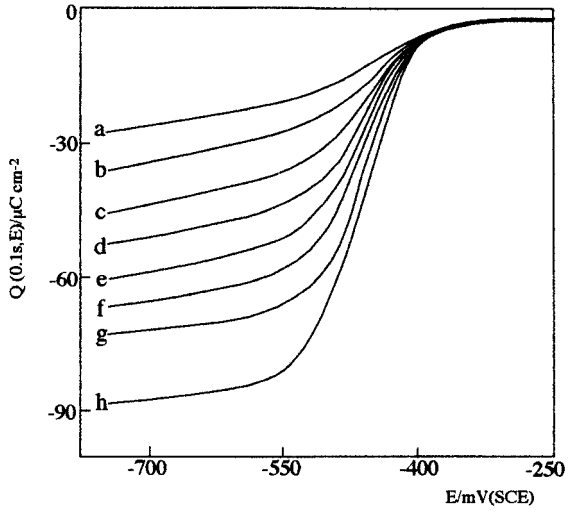

FIGURE 3 Plots of the chronocoulometric charge $Q(t = 0.1$ s, $E)$ for 4×10^{-4} M Tl^+ electroreduction on DOPS-coated mercury from buffered aqueous solutions of 0.1 M KCl + 1.5×10^{-7} M GR against E. pH: (*a*) 1.90, (*b*) 2.23, (*c*) 2.64, (*d*) 3.00, (*e*) 3.28, (*f*) 3.68, (*g*) 4.46. Curve *h* is the Tl^+ wave on bare mercury.

Tl^0(Hg) electrooxidation on Tl amalgam coated with a GR-modified DOPC monolayer is not appreciably affected by such a coating, and practically coincides with the corresponding curve *d* on bare Tl amalgam.

The partitioning of 1.5×10^{-7} M GR from the aqueous solution into the lipid monolayer causes an appreciable increase in the differential capacity C. Thus, the C versus E curve attains a minimum of 3 μF cm^{-2} at ~ -0.55 V and increases exponentially on both sides of the minimum, reaching a value of ~ 7 μF cm^{-2} at -0.250 V. The increase in C is due to the polarizable water-filled GR channels. The strong potential dependence of C is quite probably to be ascribed to the presence of water molecules interposed between the lipid monolayer and the mercury surface. The high orientational polarizability of water molecules may have such an effect if the electric field experienced by them varies appreciably with a change of the applied potential. This is possible if the water molecules are in direct contact with the electrode surface.

Incorporating 23 mol% KC in the GR-modified DOPC monolayer causes an appreciable drawing out of the *i* versus *E* curve for Tl^+ electroreduction, as shown by the solid curve *c* in Fig. 1. In contrast, the plateau of the curve remains substantially unaltered. The presence of 23 mol% KC also affects the *i* versus *E* curve for Tl^0(Hg) electrooxidation, albeit to a lower extent, as shown by the solid curve *e* in Fig. 1. Thus, it causes a positive shift in its half-wave potential by $\sim$20 mV. KC creates a dipole potential positive toward the hydrocarbon tails of the lipid monolayer (Franklin and Cafiso, 1993; Gross et al., 1994), phloretin is known to create a dipole potential in the opposite direction (Andersen et al., 1976; Melnik et al., 1977; Pohl et al., 1997). The incorporation of phloretin from a 1×10^{-6}-M solution of this lipophilic sterol affects neither the *i* versus *E* curve for Tl^+ electroreduction nor that for Tl^0(Hg) electrooxidation to an appreciable extent.

The plateau of the wave for Tl^+ electroreduction is affected by the nature of the phospholipid monolayer (Nelson and Bizzotto, 1999), and also by its charge. Thus, the height of the sigmoidal curve of the chronocoulometric charge $Q(t, E)$ at constant $t = 0.1$ s against E on a DOPS-coated mercury electrode incorporating GR decreases rapidly with a decrease in pH from 6.5 to 1.90, as shown in Fig. 3, due to the progressive passage from a negative to a positive charge on the polar heads of DOPS. This decrease is accompanied by a positive shift in the half-wave potential by $\sim$35 mV. Conversely, a decrease in pH at a DOPC-coated mercury electrode incorporating GR causes a slight decrease in the plateau of the wave for Tl^+ electroreduction, at least as long as DOPC remains neutral. A more appreciable decrease is observed at pH values <2.5, when DOPC starts to become positively charged (see below).

DISCUSSION

The electroreduction behavior of Tl^+ on lipid-coated Hg and the electrooxidation behavior of Tl^0(Hg) on lipid-coated Tl amalgam in the presence of GR can be explained quantitatively on the basis of a simple kinetic model consisting of five basic steps: 1) diffusion of Tl^+ in the aqueous

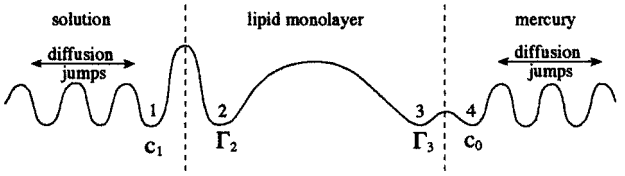

FIGURE 4 Schematic picture of the potential energy profile for Tl^+ electroreduction and Tl^0(Hg) electrooxidation through GR channels incorporated in a lipid monolayer self assembled on mercury.

solution to and from the channel mouth; 2) dehydration or hydration of Tl^+ ion at a binding site near the channel mouth; 3) translocation from the binding site to the position immediately preceding the charge-transfer step yielding Tl^0(Hg), or vice versa; 4) charge-transfer step; 5) diffusion of Tl^0(Hg) within the amalgam from or to the opposite channel mouth. Figure 4 shows schematically the potential energy profile with the associated energy barriers. Site 1 is occupied by Tl^+ just before the dehydration step, with a volume concentration c_1; site 2 is occupied by the partially dehydrated Tl^+ ion just before the translocation step, with a surface concentration Γ_2; site 3 is occupied by the partially dehydrated Tl^+ ion just before the charge-transfer step, with a surface concentration Γ_3; site 4 is occupied by Tl^0(Hg) in the amalgam adjacent to the channel mouth facing the electrode surface, with a volume concentration c_0. The rate constants for the intermediate, nondiffusional steps are defined as

$$(Tl^+)_1 + GR \underset{k_{-1}}{\overset{k_1}{\rightleftharpoons}} (Tl^+)_2 \underset{k_{-2}}{\overset{k_2}{\rightleftharpoons}} (Tl^+)_3 \overset{E^0}{\leftrightarrow} (Tl^0)_4. \quad (1)$$

k_1 is a pseudo-first-order rate constant, because it incorporates the surface concentration of GR in the lipid monolayer. $E^0 = -0.463$ V is the formal potential of the Tl^+/Tl^0(Hg) couple. In view of the very high rate at which Tl^+ ions are known to be electroreduced to Tl^0(Hg) on bare mercury (Agarwal, 1974), the charge-transfer step will be regarded as in quasi-equilibrium. To simplify notations, all potentials in the following will be referred to the formal potential E^0.

Let us denote by ϕ the potential difference across the whole mercury/solution interphase. The potential difference between the bulk aqueous phase and the surface of a DOPC monolayer can be regarded as negligible in the presence of 0.1 M KCl. This supporting electrolyte reduces the resistance of the solution around the mercury drop to ~200 Ω, and the corresponding ohmic drop to <1 mV, even at the highest currents attained in the present measurements. Moreover, the absolute value of the charge density σ_M at the surface of a phospholipid-coated mercury electrode never exceeds 1 μC cm^{-2} (Moncelli et al., 1998b). Consequently, in view of the Gouy–Chapman theory, the potential difference across the diffuse layer adjacent to a neutral lipid monolayer, such as a DOPC film, is of the order of 10 mV.

Let us denote by α the fraction of the potential difference ϕ across the mercury/solution interphase that affects the charge-transfer step, namely that between site 3 and bulk mercury. Noting that ϕ differs from the applied potential E relative to E^0 by a constant, we will have

$$\Gamma_3/c_0 = K_3 \exp(\alpha f E) \quad \text{with} \quad f \equiv F/(RT), \quad (2)$$

where K_3 is a potential independent equilibrium constant. The fraction of the potential difference ϕ across the potential energy barrier for Tl^+ translocation, namely that between sites 2 and 3 in Fig. 4, will be set equal to $(1 - \alpha)$. This amounts to regarding the potential difference across the mouth of the channel, which affects the dehydration–hydration step, as vanishingly small. Such an assumption is reasonable, especially at the relatively high KCl concentration adopted in this work. Let us denote by β the fraction of the potential difference $(1 - \alpha)\phi$ affecting Tl^+ translocation toward the electrode, and by $(1 - \beta)$ the remaining fraction affecting Tl^+ translocation toward the solution. The potential dependence of the rate constants k_2 and k_{-2} will be expressed by the usual Boltzmann factors,

$$k_2 = k_2^0 \exp[-(1 - \alpha)\beta f E],$$
$$k_{-2} = k_{-2}^0 \exp[(1 - \alpha)(1 - \beta) f E], \quad (3)$$

where k_2^0 and k_{-2}^0 are rate constants at the formal potential of the Tl^+/Tl^0(Hg) couple. The treatment of this boundary value problem under steady-state conditions is outlined in Appendix A in the framework of the diffusion-layer approximation (Guidelli, 1971). According to this treatment, Tl^+ electroreduction through GR channels is controlled both by diffusion and by the potential-independent partial dehydration of the Tl^+ ion at the mouth of the ion channel, while the translocation step is substantially in quasi-equilibrium. Under these conditions the treatment predicts a positive shift in the half-wave potential for Tl^+ electroreduction with respect to the formal potential E^0 by an amount equal to $(RT/F)\ln(i_{d,c}/i_{l,c})$, where $i_{d,c}$ is the cathodic diffusion-limiting current, as recorded on bare mercury, and $i_{l,c}$ is the cathodic limiting current in the presence of the lipid monolayer incorporating GR (see Eq. A7). Under the experimental conditions of curve *b* in Fig. 1, the $i_{l,c}/i_{d,c}$ ratio equals 0.80. Hence, the treatment predicts a positive shift of 5.7 mV, in agreement with the experimental shift of ~6 mV. The rate constant k_1 for the dehydration step can be readily obtained from the simple relationship $k_1 = \sqrt{(D/\pi t)}\, i_{l,c}/(i_{d,c} - i_{l,c})$, where $D \approx 2 \times 10^{-5}$ cm^2/s is the Tl^+ diffusion coefficient in the aqueous solution (Kolthoff and Lingane, 1952) and t is the electrolysis time (see Eq. A5). From the experimental values $t = 0.1$ s and $i_{l,c}/i_{d,c} = 0.80$ in Fig. 1, a k_1 value of 0.03 cm/s is obtained. The dashed curve *b* in Fig. 1 was obtained from Eq. A7 and is in fairly good agreement with the corresponding experimental solid curve.

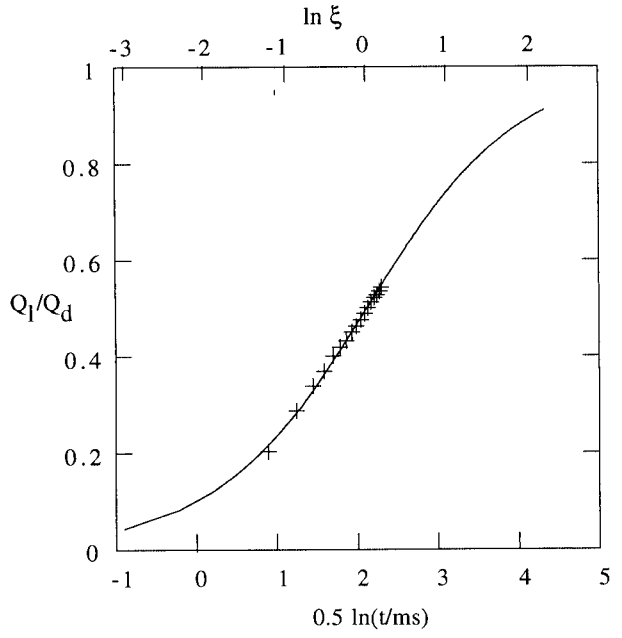

FIGURE 5 Working curve of the ratio, $Q_l(t)/Q_d(t)$, of the limiting charge, $Q_l(t)$, for Tl^+ electroreduction across GR ion channels to its diffusion limiting value, $Q_d(t)$, against ln ξ, with $\xi \equiv k_1\sqrt{(t/D)}$. Crosses are experimental values of the $Q_l(t)/Q_d(t)$ ratio against 0.5 ln t.

When the translocation step is in quasi-equilibrium, the rigorous expressions for $i(t, E)$ and $Q(t, E)$ of Eqs. A11 and A12 can be used. Figure 5 shows the working curve of the ratio, $Q_l(t)/Q_d(t)$, of the limiting charge, $Q_l(t)$, for Tl^+ electroreduction through GR channels to its diffusion-limiting value, $Q_d(t)$, as a function of ln ξ, with $\xi \equiv k_1\sqrt{(t/D)}$. This curve was calculated from Eq. A12 under limiting charge conditions, i.e., for $E \rightarrow \infty$. The figure also reports the experimental values of the $Q_l(t)/Q_d(t)$ ratio versus 0.5 ln t, with t in ms. The two horizontal axes, ln ξ and 0.5 ln t, were shifted with respect to each other to provide the best overlapping between the two curves. Under these conditions, the ln $\xi = 0$ value lies on the same vertical axis as the 0.5 ln $t = +2.1$ value. This implies that $k_1\sqrt{(t/D)}$ equals unity for $t = 66.7 \times 10^{-3}$ s, and hence that k_1 is about equal to 1.7×10^{-2} cm/s, once we set $D = 2 \times 10^{-5}$ cm^2/s. This value is about one half that obtained by the approximate procedure. It was used in Eq. A12 to calculate the potentiostatic $Q(t, E)$ versus time curves for different values of $E - E_{1/2}$, where $E_{1/2} = -0.457$ V is the half-wave potential of the experimental $Q(t, E)$ versus E curve at constant t for Tl^+ electroreduction on DOPC-coated mercury in the presence of 1.5×10^{-7} M GR. Figure 2 shows both the experimental and the calculated $Q(t, E)$ versus t curves. Agreement is again satisfactory.

The k_1 value for the 1.5×10^{-7} M GR concentration is a pseudo-first-order rate constant, which must be multiplied by the surface concentration, Γ_{GR}, of the GR channels in the lipid monolayer to provide the second-order ion-channel entry rate constant. Unfortunately, the adsorption isotherm relating Γ_{GR} to the GR concentration in the aqueous solution is unknown. It was assumed by Wallace (1996) that the interaction of Tl^+ ions with GR dimers spanning lipid bilayers is similar to that with GR monomers spanning lipid monolayers. On the basis of this reasonable assumption, a rough estimate of the Γ_{GR} value in equilibrium with the 1.5×10^{-7} M GR bulk concentration adopted in the present measurements can be obtained upon dividing $k_1 = 1.7 \times 10^{-2}$ cm/s by the value of the second-order rate constant, $k_{in} = 5 \times 10^{11}$ mol^{-1}cm^{3}s^{-1}, obtained by Urban et al. (1980) for Tl^+ entry into the GR dimeric channel. This yields $\Gamma_{GR} = 3.4 \times 10^{-14}$ mol cm^{-2}, in good agreement with the maximum value, 3.8×10^{-14} mol cm^{-2}, estimated by Nelson and Bizzotto (1999) on the basis of similar assumptions. With this Γ_{GR} value, the average distance between GR channels, assumed to be distributed on a hexagonal lattice, equals $(\sqrt{3}N_{Av}\Gamma_{GR}/2)^{-1/2} = 7.5 \times 10^{-6}$ cm, where N_{Av} is the Avogadro number. This distance is much shorter than the diffusion layer thickness, $\delta = \sqrt{(\pi Dt)} = 2.5 \times 10^{-4}$ cm, attained after 1 ms from the instant of the potential jump. This excludes the possibility for the plateau of the Tl^+ wave to be influenced by radial diffusion of Tl^+ ions toward single GR channels. It should be noted that limiting currents under radial diffusion conditions are predicted to be lower than those under linear diffusion conditions (Amatore et al., 1983); hence, a regime of radial diffusion would justify, at least partially, the $i_{l,c}$ value for the Tl^+ wave being less than $i_{d,c}$.

That radial diffusion is to be excluded is also supported by the experimental observation that the limiting current of the Tl^0(Hg) oxidation wave on lipid-coated Tl amalgam incorporating GR is exclusively controlled by linear diffusion. This experimental behavior agrees with the prediction of Eq. A10, which expresses the Tl^0(Hg) oxidation wave when the translocation step is in quasi-equilibrium. The limiting current for Tl^0(Hg) oxidation wave, being diffusion controlled, implies that the hemispherical diffusion layers initially formed by the Tl^0 atoms diffusing toward the inner mouth of the individual GR channels merge into a single planar diffusion layer much before the time interval covered by the present chronocoulometric measurements. It also implies that the rate constant k_{-1} for the hydration of the Tl^+ ions resulting from Tl^0(Hg) electrooxidation is much lower than that, k_2^0, for Tl^+ translocation.

Evidence in favor of a partial control of the limiting current $i_{l,c}$ for Tl^+ electroreduction by the dehydration step is also provided by the influence exerted upon $i_{l,c}$ by the charge on the polar heads of lipid monolayers. Figure 6 shows plots of the dehydration rate constant k_1 versus pH for Tl^+ electroreduction on DOPC- and DOPS-coated mercury, over the pH range from 1.9 to 6.6. These k_1 values were calculated from experimental values of the Q_l/Q_d ratio at $t = 0.1$ s by using the working curve in Fig. 5 and setting $D = 2 \times 10^{-5}$ cm^2/s, as usual. The dehydration rate

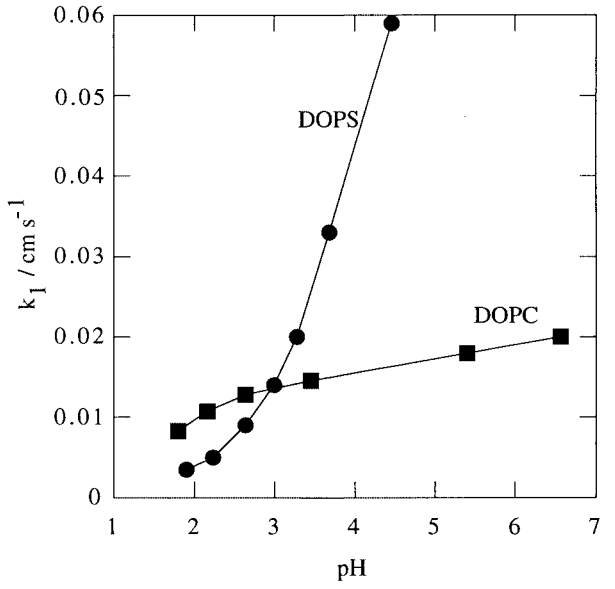

FIGURE 6 Plots of the dehydration rate constant k_1 against pH for Tl^+ electroreduction on DOPC- and DOPS-coated mercury from buffered aqueous solutions of 0.1 M KCl + 1.5×10^{-7} M GR.

constant on DOPC monolayers decreases slowly with decreasing pH up to pH 2.5; a more rapid decrease is observed over the pH range from 2.5 to 1.8, when DOPC starts to become positively charged (Moncelli et al., 1994). This behavior is explained by a progressive electrostatic repulsion of the Tl^+ ions from the lipid surface. This causes a decrease in the Tl^+ volume concentration c_1 at the mouth of the GR channels, with a resulting decrease in the limiting current $i_{l,c}$. A much greater decrease in $i_{l,c}$ with a decrease in pH is observed on a DOPS monolayer. It was shown from differential capacity measurements that a gradual decrease in pH causes the charge of a self-assembled DOPS monolayer on mercury to pass from negative to positive values at a pH of ~6 (Moncelli et al., 1994). If the effect of the nature of the phospholipid film on $i_{l,c}$ were exclusively electrostatic, we should conclude that, under the present conditions, the DOPS film becomes neutral at the intersection point of the two curves in Fig. 6, at a pH of ~3, because DOPC is almost neutral at this pH. However, specific effects due to the different nature of the polar heads of DOPC and DOPS cannot be ruled out. In particular, it is possible that the GR channels may induce conformational changes in the neighboring DOPS polar heads, with a resulting increase in their acidity; conformational changes of the DOPS polar heads having such an effect were actually postulated (Moncelli et al., 1994).

In comparing the present results with those obtained on neutral BLMs (mainly glyceromonooleate membranes), some points must be stressed. Although both biomimetic systems rely on models for the interpretation of experimental results, the results obtained on BLMs are more model dependent and involve a higher number of adjustable parameters. This is particularly true if double occupancy (Urban et al., 1980), or even triple occupancy (Levitt, 1978), is accounted for. In certain models, four bonding sites (two at each end) have been included (Eisenman and Sandblom, 1976; Sandblom et al., 1977; Hladky, 1984). Hladky et al. (1979) and Urban et al. (1980) have assumed in their models that the entry and exit steps are also potential dependent, with a resulting increase in the number of adjustable parameters. In addition, fitting these models to Tl^+ conductance has often been found more difficult and less satisfactory than fitting them to the conductance of alkali metal ions (Levitt, 1978; Urban, 1980). Usually, all these models yield a relatively high value for the second-order entry rate constant k_{in}: 11.8×10^{-16} liters/s (Levitt, 1978); 9×10^{-16} liters/s (Urban, 1980); 4×10^{-16} liters/s (Andersen, 1978). The latter value was obtained by Andersen from the limiting conductance at high voltage, which requires a lower number of adjustable parameters for its fitting. Slightly lower k_{in} values were obtained by Andersen (1983) for alkali metal ions. Other rate constants, such as the rate constant k_2^0 for Tl^+ translocation across the GR channel, appear to be much more model dependent (Levitt, 1978; Urban et al., 1980), also in view of the different voltage dependence ascribed to the translocation step in different models. The high k_{in} value, for which substantial agreement exists in the literature, has been regarded as evidence for probable (Levitt, 1978; Hladky, 1984) or sure (Andersen, 1983) diffusion control. Indeed, all four maneuvers used by Andersen (1983) to change the aqueous diffusion coefficient of the permeant ions show unequivocally that the voltage-independent rate constant k_{in} varies in a manner qualitatively consistent with a diffusion-controlled entry step. However, establishing unambiguously that the entry step is "exclusively" controlled by diffusion on the basis of single-channel current measurements is a prohibitive task. In fact, the diffusion equations predicting the rate at which ions can enter a narrow pore are roughly approximate (Hladky, 1984). The classical expression for steady-state diffusion to a hemispherical surface is (Andersen and Feldberg, 1996)

$$J = D(c_1^* - c_1)/r_0. \quad (4)$$

Here J is the ion flux, c_1 and c_1^* are the ion concentrations at the channel entrance and in the bulk solution, and D is the bulk diffusion coefficient. Moreover, r_0 is the capture radius, which is defined as the difference between the luminal radius of the channel and the relevant radius of the permeant ion (Läuger, 1976). The capture radius has been ascribed values ranging from 0.2 (Andersen, 1983) to 1 Å (Levitt, 1978). In addition, the effective diffusion coefficient of ions close to the channel entrance may be appreciably lower than its bulk value (Andersen, 1983). For the above reasons, the value of the maximum limiting ion flux, $J_{max} = Dc_1^*/r_0$, as attained when the volume concentration c_1 at the channel mouth vanishes, can be estimated only approximately.

Some deviations of experiment from the predictions of a purely diffusion-controlled process (Andersen, 1983) led Andersen and Feldberg (1996) to assume a partial control of the ion flux to the channel mouth by collisional rate. To this end, they combined the expression of Eq. 4 for a purely diffusional flux with that, $J = v_0 c_1$, for a collision-controlled flux. The resulting expression is such that at high voltages, when the incoming ions translocate across the channel instantaneously after their collision with the hemispherical channel mouth, the volume concentration c_1 at the channel mouth is no longer equal to zero, but assumes the steady-state value,

$$c_1 = c_1^* \left[1 - 1 \Big/ \left(1 + \frac{D}{v_0 r_0} \right) \right].$$

Once it is assumed that c_1 does not vanish at sufficiently high voltages, it becomes difficult to establish whether this is due to partial control by the collisional rate of the permeant ion or by its partial dehydration rate. The latter hypothesis was excluded by Andersen and Feldberg (1996) on the basis of the consideration that a slow dehydration step would cause the limiting current to be independent of the bulk concentration of the permeant ion. As a matter of fact, this conclusion holds only if the channel mouth facing the solution is permanently occupied by the permeant ion. Regarding the occupation of the outer mouth of the channel by the permeant ion as an adsorption process, a fast translocation of the ion across the channel may well maintain the adsorption isotherm within the linear (Henry) isotherm region even at relatively high bulk concentrations of the ion. It is, therefore, difficult to discriminate between collisional rate and partial dehydration rate as the cause of a nonzero c_1 value at high voltages. However, the limiting current for Tl^0(Hg) electrooxidation across a GR-modified DOPC monolayer (curve *e* in Fig. 1), being diffusion controlled, suggests that the entry rate constant for Tl^+ electroreduction is the result of a dehydration step. In fact, a collisional rate would also partly control the entry of Tl^0 atoms into the GR channel mouth facing the Tl amalgam surface.

The multichannel measurements carried out with the present biomimetic membrane present a number of advantages over single-channel measurements: 1) their sensitivity is higher due to the much higher currents involved; 2) the low Tl^+ concentrations adopted in view of the high sensitivity and the very high rate of the $Tl^+ \rightarrow Tl^0$(Hg) electron-transfer step exclude the occupancy of the channel mouth facing the mercury surface, at least under limiting current conditions; therefore, under these conditions the current depends exclusively upon the single adjustable parameter k_1; 3) the laws of linear diffusion are well established and do not require adjustable parameters, as opposed to the diffusion equations toward the mouth of a narrow channel; 4) the limiting current of Tl^+ ions across GR channels incorporated in a mercury-supported phospholipid monolayer can be directly compared with the corresponding diffusion-limiting current on a bare mercury electrode, under otherwise identical experimental conditions. Such a comparison shows unequivocally that Tl^+ diffusion toward the GR channels incorporated in a neutral phospholipid monolayer plays a major, but not exclusive, role in controlling the limiting current; partial control by ion dehydration rate (and possibly, to a minor extent, by collisional rate) is also operative. This control tends to increase progressively, and ultimately to prevail over diffusion control, as the charge of the phospholipid monolayer becomes increasingly positive, as appears from Figs. 3 and 6.

A drawback of the present measurements with respect to single-channel measurements is represented by the impossibility of estimating the surface density of the GR channels incorporated in the lipid. What is measured is an average current over a very high number of channels and over time. In this respect, the average number of active channels responsible for the mean current may be less than the number of channels actually incorporated in the lipid film, if the GR monomers fluctuate between conducting and nonconducting states. Therefore, the entry rate constant k_1 derived from these measurements is a pseudo-first-order rate constant, and cannot be compared with the second-order rate constant k_{in} obtained from single-channel measurements.

The drawing out of the Tl^+ reduction wave (solid curve *c* in Fig. 1) and the positive shift of the Tl^0(Hg) oxidation wave (solid curve *e* in Fig. 1) caused by incorporation of 23 mol% KC in the GR-modified DOPC monolayer are explained by the effect of the KC dipole potential upon the translocation step. The KC molecule has the dipole moment, due primarily to its carbonyl group, with the negative end (the oxygen atom) turned toward the aqueous solution. This contributes to increasing the potential energy barrier for the translocation of the partially dehydrated Tl^+ ion in both directions. The resulting decrease in the rate constant k_2^0 for the translocation step causes this step to contribute to the kinetics of the overall process along the rising portion of the Tl^+ and Tl^0(Hg) waves. Naturally, at sufficiently negative potentials for the Tl^+ wave, and at sufficiently positive potentials for the Tl^0(Hg) wave, the translocation step is so strongly assisted by the electric field that it ceases determining the rate of the overall process. Hence, the limiting currents $i_{l,c}$ and $i_{l,a}$ are not affected by the dipole potential of KC. The Tl^+ wave on DOPC-coated mercury incorporating KC and GR (solid curve *c* in Fig. 1) and the Tl^0(Hg) wave on DOPC-coated Tl amalgam incorporating KC and GR (solid curve *e* in Fig. 1) can be satisfactorily interpreted on the basis of the general Eqs. A6 and A9, which account for simultaneous control by diffusion, hydration–dehydration, and translocation steps. Thus, the dashed curves *c* and *e* in Fig. 1 are Tl^+ and Tl^0(Hg) current versus potential curves calculated from these equations by setting $i_{l,c}/i_{d,c} = 0.8$, $(1 - \alpha)\beta = 0.25$ and $k_{-1}/k_2^0 = 4$. The $(1 - \alpha)\beta$ factor being <0.5 accounts for the Tl^+ wave having a more sloping

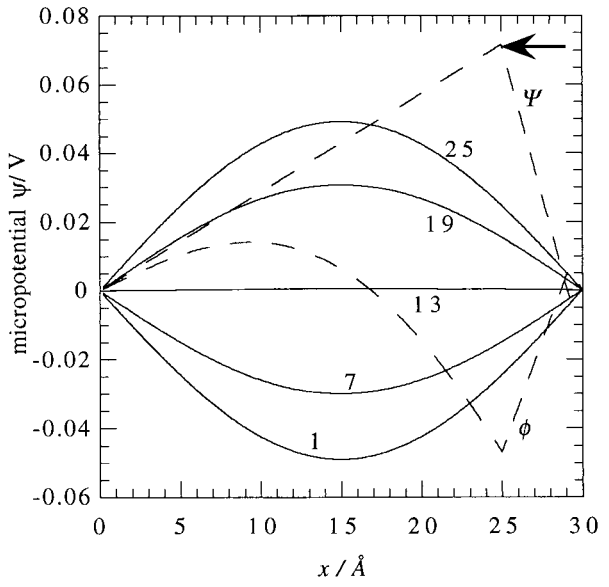

FIGURE 7 Plots of the micropotential created by a layer of dipoles of length $l = 4.2$ Å and magnitude 2.4 D along the axis of a cylindrical ion channel, 2 Å in radius, as a function of the distance x from the electrode surface plane. The positive poles are at a distance $x = b$, the negative ones at a distance $x = b + l$. The plots were calculated for a length $d = 30$ Å of the lipid monolayer and for a dielectric constant $\varepsilon = 4$. Numbers on the different solid curves are b values, in Å. The dashed curves express the macropotential $\Psi(x)$ and the disk potential, $\phi_b(x) + \phi_{b+l}(x)$, for the case of $b = 25$ Å.

rising section than the Tl^0(Hg) wave, and can be justified by a region of the potential energy barrier for ion translocation that does not extend throughout the whole length of the lipid monolayer.

The increase of the potential energy barrier for ion translocation produced by the dipole potential of the KC molecules is estimated in Appendix B by a cut-off disk model with perfect imaging of nonideal dipoles of KC both in the metal surface plane, $x = 0$, and in the lipid/solution boundary, $x = d$. The model allows the calculation of the profile of the local potential ψ (the so-called micropotential) created by the KC dipoles along the axis of the ion channel. Franklin and Cafiso (1993) estimated the length of the component of a KC molecule incorporated in a phosphatidylcholine bilayer in the direction normal to the bilayer at about $l = 4.2$ Å and its magnitude at 2.4 D, with the negative end turned toward the solution. Upon ascribing to the KC and DOPC molecules cross-sectional areas of 45 and 65 $Å^2$, respectively, 23 mol% KC in the DOPC monolayer creates a charge density $\sigma_i = 4.5 \times 10^{-4}$ e/$Å^2$ on the ideal plane containing the positive poles of the KC molecules, at a distance b from the electrode surface plane, and an equal and opposite charge density $-\sigma_i$ on the ideal plane containing the negative poles, at a distance $b + 4.2$ Å from the electrode surface plane. Figure 7 shows plots of the micropotential created by the KC nonideal dipoles along the axis of a cylindrical ion channel, 2 Å in radius, as a function of the distance x from the electrode surface plane. The plots were calculated for a length $d = 30$ Å of the phospholipid monolayer and for a dielectric constant $\varepsilon = 4$. Numbers on the different solid curves refer to the distance, $x = b$, of the positively charged plane from the electrode surface. It is apparent that the KC dipoles create a true barrier to cation translocation only if they are located close to the lipid/water boundary, $x = d$. As the dipoles are shifted toward the metal surface plane, the barrier height first decreases, then vanishes in the middle of the lipid monolayer, and ultimately evolves into a depression, at still shorter distances from the metal surface plane. In all cases, the maximum (or minimum) of the profile lies in the middle of the lipid monolayer. This behavior is due to the different extent of the screening of the two poles of the nonideal KC dipoles by their infinite images. When the negative poles are almost in contact with $x = d$ (*arrow* in Fig. 7), they are much more effectively screened than are their positive counterparts; hence, the translocating cation will especially experience the repulsion by the positive poles. Conversely, when the positive poles are almost in contact with the metal surface plane, $x = 0$, they will be more effectively screened than are their negative counterparts, and the translocating cation will especially experience the attraction by the negative poles. Repulsive and attractive effects of the two poles compensate each other in the middle of the lipid monolayer. The values of the maxima or minima of the micropotential profiles depend critically upon the value ascribed to the dielectric constant. If the ion channel and the lipid in contact had both a semi-infinite extension, the electrostatic effect that the charges in the lipid exert inside the channel would be adequately represented by the average, $(\varepsilon_{lip} + \varepsilon_{chan})/2$, of the dielectric constants of the lipid and the channel (Jackson, 1975). Tredgold and Hole (1976) measured the dielectric constant of dry polypeptides in β-pleated conformations. They found that the dielectric constant varied between 4 and 25. In contrast, the dielectric constant of the hydrocarbon tails of a lipid is ~2, whereas that of the polar heads is more uncertain, having been ascribed values ranging from 8 (Lelkes and Miller, 1980) to 30 (Flewelling and Hubbell, 1986). An average dielectric constant of 4, such as that used in Fig. 7, is therefore reasonable. If the KC dipoles are in close proximity of the lipid/solution interface, they are therefore expected to decrease the rate constant k_2^0 for the translocation step by the Boltzann factor $\exp(-F\psi/RT) \cong 0.143$, where ψ was set equal to its maximum value, 50 mV, in Fig. 7.

In conclusion, the present results show that the approximately potential independent-limiting flux of hydrated Tl^+ ions through GR channels incorporated in phospholipid monolayers supported by mercury is controlled both by diffusion and by a dehydration step. Conversely, the potential independent-limiting flux of dehydrated Tl^+ ions stemming from Tl amalgam eletrooxidation is exclusively con-

trolled by diffusion. The modulation of the charge on the polar heads of DOPS carried out by changing pH affects the limiting flux of hydrated Tl^+ ions to a notable extent, primarily by electrostatic interactions. The dipole potential of DOPS and DOPC, positive toward the hydrocarbon tails, does not hinder the translocation step of Tl^+ ions to such an extent as to make it partially rate determining. Consequently, incorporation in the lipid monolayer of phloretin, which decreases such a positive dipole potential, does not affect the kinetics of Tl^+ flux through the GR channel. In contrast, the increase in the positive dipole potential produced by the incorporation of KC causes the translocation step to contribute to the rate of the overall process.

APPENDIX A

Under steady-state conditions, the current i is given by

$$i/(FA) = k_1c_1 - k_{-1}\Gamma_2 = k_2\Gamma_2 - k_{-2}\Gamma_3 = k_2\Gamma_2 - k_{-2}K_3c_0\exp(\alpha fE), \quad \text{(A1)}$$

in view of Eq. 2. Here, A is the electrode area. A relationship between the various rate constants is obtained by applying the equilibrium condition,

$$\frac{c_1}{\Gamma_2}\frac{\Gamma_2}{\Gamma_3}\frac{\Gamma_3}{c_0} = \frac{k_{-1}}{k_1}\frac{k_{-2}}{k_2}K_3\exp(\alpha fE) = \exp(fE) \quad \text{with} \quad f \equiv F/(RT). \quad \text{(A2)}$$

Here, the applied potential E is referred to the formal potential E^0 of the Tl^+/Tl^0(Hg) couple. Rearranging terms in Eq. A1, eliminating $k_{-2}K_3$ via Eq. A2, and accounting for the potential dependence of k_2 via Eq. 3, we get

$$\frac{i}{FA} = \frac{k_1k_2^0\exp[-(1-\alpha)\beta fE]}{k_2^0\exp[-(1-\alpha)\beta fE] + k_{-1}}[c_1 - c_0\exp(fE)]. \quad \text{(A3)}$$

Let us now account for the diffusion steps for the case of Tl^+ electroreduction in the absence of Tl^0(Hg) in the bulk mercury. According to the diffusion-layer approximation (Guidelli, 1971), we have

$$c_1 = c_1^*(i_d - i)/i_d, \quad c_0 = c_1^*i/i_d. \quad \text{(A4)}$$

Here, c_1^* is the Tl^+ concentration in the bulk solution and $i_{d,c} = FADc_1^*/\delta$ is the cathodic diffusion-limiting current, where D is the diffusion coefficient of Tl^+ and $\delta = \sqrt{(\pi Dt)}$ is the diffusion layer thickness at the electrolysis time t. Substituting c_1 and c_0 from Eq. A4 into Eq. A3 and letting E tend to $-\infty$ in the resulting current-potential characteristic, we obtain the limiting current $i_{l,c}$ for Tl^+ electroreduction through the ion channel,

$$i_{l,c}/i_{d,c} = k_1/(k_1 + D/\delta) \quad \text{with} \quad \delta \equiv \sqrt{\pi Dt}. \quad \text{(A5)}$$

Substituting k_1 from Eq. A5 into such a current-potential characteristic and rearranging terms, we obtain the final expression of i as a function of E for Tl^+ electroreduction,

$$\frac{i}{i_{l,c}} = \exp[-(1-\alpha)\beta fE] \div \{\exp[-(1-\alpha)\beta fE] \cdot [\exp(fE)i_{l,c}/i_{d,c} + 1] + (k_{-1}/k_2^0)(1 - i_{l,c}/i_{d,c})\}. \quad \text{(A6)}$$

This expression is only a function of the parameter $(1-\alpha)\beta$ and of the ratio, k_{-1}/k_2^0, of the rate constants of the two unidirectional steps that consume the partially dehydrated Tl^+ ion in position 2. If $k_2^0 \gg k_{-1}$, the translocation step is in quasi-equilibrium, and the current-potential characteristic assumes the simple form,

$$E = -\frac{RT}{F}\ln\left(\frac{i}{i_{l,c} - i}\right) + \frac{RT}{F}\ln\left(\frac{i_{d,c}}{i_{l,c}}\right). \quad \text{(A7)}$$

This equation has the same form as that for a reversible, diffusion-controlled Tl^+ wave on bare mercury. The only difference is represented by the fact that the limiting current $i_{l,c}$ is now lower than the corresponding diffusion-limiting value, $i_{d,c}$, being partially controlled by the rate of the dehydration step (see Eq. A5). Moreover, the half-wave potential (i.e., the potential at which $i = i_{l,c}/2$) is shifted positively with respect to the formal potential of the Tl^+/Tl^0(Hg) couple by an amount equal to $(RT/F)\ln(i_{d,c}/i_{l,c})$. Naturally, if k_1 is much greater than D/δ, which is a measure of the diffusion rate, then Eq. A5 shows that $i_{l,c}$ tends to $i_{d,c}$, and the reduction wave of Tl^+ through the ion channel comes to coincide with the reversible, diffusion-controlled wave on bare mercury.

To account for the diffusion steps in the case of Tl^0(Hg) electrooxidation in the absence of Tl^+ in the bulk solution, the starting point is again Eq. A3. According to the diffusion-layer approximation (Guidelli, 1971), we now have

$$c_0 = c_0^*(i_{d,a} - i)/i_{d,a}, \quad c_1 = c_0^*i/i_{d,a}. \quad \text{(A8)}$$

Here, c_0^* is the Tl^0 concentration in the bulk amalgam and $i_{d,a} = FADc_0^*/\delta$ is the anodic diffusion limiting current. For simplicity, the diffusion coefficient of Tl^0 in the amalgam will be set equal to that of Tl^+ in the solution. Substituting c_0 and c_1 from Eq. A8 into Eq. A3 and letting E tend to $+\infty$ in the resulting current-potential characteristic, we obtain an anodic-limiting current $i_{l,a}$ for Tl^0(Hg) electrooxidation through the ion channel, which coincides with its diffusion-limiting value, $i_{d,a}$. This is not surprising, because, in the present case, charge transfer is not preceded by a chemical step. Rearranging terms and expressing the rate constant k_1 via Eq. A5 as a function of the cathodic-limiting current $i_{l,c}$ derived from independent measurements, we obtain the current-potential characteristic,

$$\frac{i}{i_{d,a}} = \exp\{[1-(1-\alpha)\beta]fE\} \div \{\exp[-(1-\alpha)\beta fE] \cdot [\exp(fE) + i_{d,c}/i_{l,c}] + (k_{-1}/k_2^0)(i_{d,c}/i_{l,c} - 1)\}. \quad \text{(A9)}$$

This is again a function of the parameter $(1-\alpha)\beta$ and of the k_{-1}/k_2^0 ratio. For $k_2^0 \gg k_{-1}$, Eq. A9 simplifies as

$$\frac{i}{i_{d,a}} = \frac{\exp(fE)}{\exp(fE) + i_{d,c}/i_{l,c}}. \quad \text{(A10)}$$

If, in addition, $k_1 \gg D/\delta$, Eq. A10 reduces to the reversible, diffusion-controlled wave for Tl^0(Hg) electroxidation on bare amalgam.

A rigorous expression for potentiostatic current versus time curves in the case of a Nernstian electron transfer preceded by a heterogeneous chemical step was derived by one of the authors (Guidelli, 1968). It can be applied to Tl^+ electroreduction through GR channels when the translocation step is in quasi-equilibrium, i.e., for $k_2^0 \gg k_{-1}$. If the species undergoing the preceding chemical step is only slightly adsorbed, this expression takes the simplified form [Eq. 20 in Guidelli (1968) with a^*, $b^* = 0$, $l = 1$, and $K\rho = k_1$],

$$\frac{i(t,E)}{FA} = \frac{k_1c_1^*}{1 + \exp[f(E - E_{1/2})]}\exp(\xi^2)\mathrm{erfc}(\xi) \quad \text{with} \quad \xi \equiv k_1\sqrt{t/D}. \quad \text{(A11)}$$

Here, $E_{1/2}$ is the half-wave potential, namely the potential at which the current is one half of its limiting value. Integrating Eq. A11 over time to

obtain the corresponding expression for the charge $Q(t, E)$, and noting that the diffusion-limiting value of $Q(t, E)$ is given by the Cottrell equation, $Q_d(t) = 2FAc_1^*\sqrt{(Dt/\pi)}$, we get

$$\frac{Q(t,E)}{Q_d(t)} = \frac{\pi^{1/2}}{2\xi\{1+\exp[f(E-E_{1/2})]\}} \times \left[\exp(\xi^2)\mathrm{erfc}(\xi) + \frac{2}{\pi^{1/2}}\xi - 1\right]. \quad \text{(A12)}$$

APPENDIX B

The presence of an array of oriented dipoles within the lipid monolayer makes an electrostatic contribution to the potential energy barrier for ion translocation. The electric potential experienced by the translocating ion is a local potential ψ (the so-called micropotential). This can be estimated on the basis of the cut-off disc model (Levine et al., 1962; Moncelli et al., 1995). According to this model, the positive poles of the dipole array, at a distance $x = b$ from the electrode surface plane, $x = 0$, are considered to be smeared out on a plane of charge density σ_i; the same procedure is adopted for the negative poles, at a distance $x = b + l$, where l is the length of the dipoles. The ion channel cuts out two circular charge-free regions (the so-called exclusion disks) from the two charged planes $x = b$ and $x = b + l$, of charge densities σ_i and $-\sigma_i$. These charge-free regions are created by overlapping on each of the two charged planes one disk of opposite charge density and with the same radius a as the ion channel. The above charge distributions are imaged both in the metal surface plane, $x = 0$, and in the lipid monolayer–solution boundary, $x = d$. Perfect "conducting-conducting" imaging conditions will be assumed. The micropotential $\psi(x)$ along the axis of the ion channel will, therefore, be given by the average potential, $\Psi(x)$, created by the two infinite planar charge distributions (the so-called macropotential), plus the potential, ϕ, created by the two charged disks of opposite sign. The expression for $\Psi(x)$ is obtained by considering that the two infinite planar charge distributions and their infinite images must have no effect on the two conducting planes $x = 0$ and $x = d$, because they have, alternatively, charge densities σ_i and $-\sigma_i$, and hence their electric fields cancel each other on the $x = 0$ and $x = d$ planes. This result is achieved by locating a fictitious charge density σ_M on the $x = 0$ plane and an opposite charge density $-\sigma_M$ on the $x = d$ plane, and by adjusting σ_M to set the potential difference between the $x = 0$ and $x = d$ planes equal to zero:

$$(4\pi/\varepsilon)[b\sigma_M + l(\sigma_M + \sigma_i) + (d - b - l)\sigma_M] = 0 \rightarrow \sigma_M = -(l/d)\sigma_i.$$

Here, ε is a dielectric constant. With the above σ_M value, the macropotential Ψ as a function of x is given by

$$\Psi(x) = \begin{cases} \dfrac{4\pi l}{\varepsilon\, d}\sigma_i x & \text{for} \quad 0 < x < b, \\ \dfrac{4\pi}{\varepsilon}\sigma_i\left[b + x\left(\dfrac{l}{d} - 1\right)\right] & \text{for} \quad b < x < b + l, \\ \dfrac{4\pi}{\varepsilon}\sigma_i l\left(\dfrac{x}{d} - 1\right) & \text{for} \quad b + l < x < d. \end{cases} \quad \text{(B1)}$$

The contribution, $\phi_b(x)$, to ϕ along the axis of the ion channel from the disk of charge density $-\sigma_i$ and radius a, located at $x = b$, and from its infinite images is given by

$$\phi_b(x) = -\sigma_i \sum_{n=-\infty}^{+\infty} \int_0^{2\pi} d\vartheta \int_0^a \left(\frac{r\, dr}{\sqrt{r^2 + (x - b - 2nd)^2}} - \frac{r\, dr}{\sqrt{r^2 + (x + b - 2nd)^2}} \right).$$

Upon carrying out algebraic manipulations and using the Poisson summation formula, the above expression takes the form

$$\phi_b(x) = -4\pi d\sigma_i \sum_{n=-\infty}^{+\infty} [F_1(n) - F_2(n)] = -4\pi d\sigma_t \sum_{y=-\infty}^{+\infty} \int_{-\infty}^{+\infty} [F_1(n) - F_2(n)]\exp(-2\pi i y n)\, dn,$$

with

$$F_1(n) \equiv \sqrt{\tau^2 + \left(n + \frac{b-x}{2d}\right)^2} - \left|n + \frac{b-x}{2d}\right|,$$

$$F_2(n) \equiv \sqrt{\tau^2 + \left(n - \frac{b+x}{2d}\right)^2} - \left|n - \frac{b+x}{2d}\right|,$$

$$\tau \equiv \frac{a}{2d}.$$

After further lengthy algebraic manipulations in which use is made of the Bessel function,

$$K_1(2\pi y\tau) \equiv \frac{\tau}{2\pi y}\int_0^\infty \frac{\cos(2\pi yz)}{(z^2 + \tau^2)^{3/2}}\, dz,$$

and of the Fourier series

$$\sum_{k=1}^{\infty}\frac{\cos kz}{k^2} = \frac{\pi^2}{6} - \frac{\pi z}{2} + \frac{z^2}{4} \quad \text{for} \quad 0 \le z \le 2\pi,$$

we obtain the final rapidly convergent series,

$$\phi_b(x) = -4\pi\sigma_i\left\{\frac{b + x - |b - x|}{2} - \frac{bx}{d} - \sum_{y=1}^{\infty}\frac{a}{\pi y}K_1\left(\frac{\pi y a}{d}\right) \times \left[\cos\left(\pi y\,\frac{b-x}{d}\right) - \cos\left(\pi y\,\frac{b+x}{d}\right)\right]\right\}. \quad \text{(B2)}$$

The micropotential along the axis of the ion channel is given by $\psi(x) = \Psi(x) + \phi_b(x) + \phi_{b+l}(x)$, where $\Psi(x)$ is given by Eq. B1 and $\phi_b(x)$ by Eq. B2; $\phi_{b+l}(x)$ expresses the contribution to $\phi(x)$ from the disk of charge density σ_i and radius a located at $x = b + l$ and by its infinite images: it is given by an expression identical with Eq. B2, apart from the replacement of b by $(b + l)$ and $-\sigma_i$ by σ_i.

This work was supported by the Ministero dell'Universitá e della Ricerca Scientifica e Tecnologica.

REFERENCES

Agarwal, H. P. 1974. Faradaic rectification method and its applications in the study of electrode processes. *In* Electroanalytical Chemistry. A. J. Bard, editor. Vol. 7. Marcel Dekker, New York. 161–271.

Amatore, C., J. M. Saveant, and D. Tessier. 1983. Charge transfer at partially blocked surfaces. A model for the case of microscopic active and inactive sites. *J. Electroanal. Chem.* 147:39–51.

Andersen, O. S. 1978. Ion transport across simple membranes. *In* Renal Function. G. H. Giebisch and E. F. Purcell, editors. Josiah Macy, Jr. Foundation, New York. 71–99.

Andersen, O. S. 1983. Ion movement through gramicidin A channels. *Biophys. J.* 41:147–165.

Andersen, O. S., and S. W. Feldberg. 1996. The heterogeneous collision velocity for hydrated ions in aqueous solutions is $\sim 10^{-4}$ cm/s. *J. Phys. Chem.* 100:4622–4629.

Andersen, O. S., A. Finkelstein, I. Katz, and A. Cass. 1976. Effect of phloretin on the permeability of thin lipid membranes. *J. Gen. Physiol.* 67:749–771.

Andersen, O. S., and R. E. Koeppe, II. 1992. Molecular determinants of channel function. *Physiol. Rev.* 72:S89–S158.

Bamberg, E., K. Noda, E. Gross, and P. Läuger. 1976. Single-channel parameters of gramicidin A, B, and C. *Biochim. Biophys. Acta.* 419: 223–228.

Becucci, L., M. R. Moncelli, R. Herrero, and R. Guidelli. 2000. Dipole potential of monolayers of phosphatidylcholine, phosphatidylserine and phosphatidic acid on mercury. *Langmuir.* 16:7694–7700.

Busath, D. D. 1993. The use of physical methods in determining gramicidin structure and function. *Annu. Rev. Physiol.* 55:473–501.

Carlá, M., M. Sastre de Vicente, M. R. Moncelli, M. L. Foresti, and R. Guidelli. 1988. Nonconventional normal pulse polarographic techniques with a static mercury electrode for applications at very low reactant concentrations. *J. Electroanal. Chem.* 246:283–296.

Eisenman, G., and J. Sandblom. 1976. Ionic selectivity, saturation, binding, and block in the gramicidin A channel: a preliminary report. *In* Metal–Ligand Interactions in Organic Chemistry and Biochemistry. B. Pullman and N. Goldblum, editors. D. Reidel Publishing Co., Dordrecht, The Netherlands.

Ermakov, Y. A., A. Z. Averbakh, A. I. Yusipovich, and S. Sukharev. 2001. Dipole potentials indicate restructuring of the membrane interface induced by gadolinium and beryllium ions. *Biophys. J.* 80:1851–1862.

Flewelling, R. F., and W. L. Hubbell. 1986. The membrane dipole potential in a total membrane potential model. *Biophys. J.* 49:541–552.

Foresti, M. L., M. R. Moncelli, and R. Guidelli. 1980. Electrode charge measurements at dropping electrodes. Part I. Back-pressure effect and measurement of changes in charge by a potential-step method. *J. Electroanal. Chem.* 109:1–14.

Franklin, J. C., and D. S. Cafiso. 1993. Internal electrostatic potentials in bilayers: measuring and controlling dipole potentials in lipid vesicles. *Biophys. J.* 65:289–299.

Gross, E., R. S. Bedlack, Jr., and L. M. Loew. 1994. Dual-wavelength ratiometric fluorescence measurement of the membrane dipole potential. *Biophys. J.* 67:208–216.

Guidelli, R. 1968. Influence of heterogeneous chemical reactions upon potentiostatic current-time curves. *J. Phys. Chem.* 72:3535–3545.

Guidelli, R. 1971. Diffusion toward planar, spherical, and dropping electrodes at constant potential. *J. Electroanal. Chem.* 33:291–302.

Herrero, R., F. Tadini Buoninsegni, L. Becucci, and M. R. Moncelli. 1998. Electron and proton transferring properties of vitamin K_1 across a self-assembled phospholipid monolayer. *J. Electroanal. Chem.* 445: 71–80.

Herrero, R., M. R. Moncelli, L. Becucci, and R. Guidelli. 1997. Adsorption and reduction kinetics of safranine T in self-assembled phospholipid monolayers deposited on mercury. *J. Electroanal. Chem.* 425:87–95.

Herrero, R., M. R. Moncelli, R. Guidelli, M. Carlá, A. Arcangeli, and M. Olivotto. 2000. Hybrid polar compounds produce a positive shift in the surface dipole potential of self-assembled phospholipid monolayers. *Biochim. Biophys. Acta.* 1466:278–288.

Hinton, J. F., J. Q. Fernandez, D. C. Shungu, W. L. Whaley, R. E. Koeppe, II, and F. S. Millett. 1988. Tl-205 nuclear magnetic resonance determination of the thermodynamic parameters for the binding of monovalent cations to gramicidins A and C. *Biophys. J.* 54:527–533.

Hinton, J. F., W. L. Whaley, D. Shungu, R. E. Koeppe, II, and F. S. Millett. 1986. Equilibrium binding constants for the group I metal cations with gramicidin-A determined by competition studies and Tl^+-205 nuclear magnetic resonance spectroscopy. *Biophys. J.* 50:539–544.

Hladky, S. B. 1984. Ion currents through pores: the roles of diffusion and external steps in determining the currents through narrow pores. *Biophys. J.* 46:293–297.

Hladky, S. B., and D. A. Haydon. 1984. Ion movements in gramicidin channels. *Curr. Top. Membr. Transp.* 21:327–372.

Hladky, S. B., B. W. Urban, and D. A. Haydon. 1979. Permeation through membrane channels. *In* Membrane Transport Processes. C. Stevens and R. W. Tsien, editors. Raven Press. New York. 89–103.

Jackson, J. D. 1975. Classical Electrodynamics. Second Edition. Wiley, New York. 147.

Jordan, P. C. 1983. Electrostatic modeling of ion pores. II. Effects attributable to the membrane dipole potential. *Biophys. J.* 41:189–195.

Killian, J. A. 1992. Gramicidin and gramicidin-lipid interactions. *Biochim. Biophys. Acta.* 1113:391–425.

Koeppe, R. E., II, and O. S. Andersen. 1996. Engeneering the gramicidin channel. *Annu. Rev. Biophys. Biomol. Struct.* 25:231–258.

Kolthoff, M., and J. J. Lingane. 1952. Polarography. Vol. 1. Interscience Publishers, New York. 95.

Läuger, P. 1976. Diffusion-limited ion flow through pores. *Biochim. Biophys. Acta.* 455:493–509.

Lecompte, M.-F., A.-C. Bras, N. Dousset, I. Portas, R. Salvayre, and M. Ayrault-Jarrier. 1998. Binding steps of apolipoprotein A-I with phospholipid monolayers: adsorption and penetration. *Biochemistry.* 37: 16165–16171.

Lecompte, M. F., and I. R. Miller. 1980. Interaction of prothrombin and its fragments with monolayers containing phosphatidylserine. 2. Electrochemical determination of lipid layer perturbation by interacting prothrombin and its fragments. *Biochemistry.* 19:3434–3438.

Lelkes, P. I., and I. R. Miller. 1980. Perturbations of membrane structure by optical probes. I. Location and structural sensitivity of merocyanine 540 bound to phospholipid membranes. *J. Membr. Biol.* 52:1–15.

Levine, S., G. M. Bell, and D. Calvert. 1962. The discreteness-of-charge effect in electric double layer theory. *Can. J. Chem.* 40:518–537.

Levitt, D. G. 1978. Electrostatic calculations for an ion channel. *Biophys. J.* 22:221–248.

Malkov, D. Y., and V. S. Sokolov. 1996. Florescent styryl dyes of the RH series affect a potential drop on the membrane/solution boundary. *Biochim. Biophys. Acta.* 1278:197–204.

Melnik, E., R. Latorre, J. Hall, and D. Tosteson. 1977. Phloretin induced changes in ion transport across lipid bilayer membranes. *J. Gen. Physiol.* 69:243–257.

Miller, I. R., and D. Bach. 1969. Structure and membrane properties of lecithin monolayers at the polarized mercury/water interface. *J. Colloid Interface Sci.* 29:250–260.

Miller, I. R., D. Bach, and M. Teuber. 1978. Effect of polymyxin B on the structure and the stability of lipid layers. *J. Membrane Biol.* 39:49–56.

Moncelli, M. R., and L. Becucci. 1997. A novel model of the hanging mercury drop electrode. *J. Electroanal. Chem.* 433:91–96.

Moncelli, M. R., L. Becucci, and R. Guidelli. 1994. The intrinsic pK_a values for phosphatidylcholine, phosphatidylethanolamine, and phosphatidylserine in monolayers deposited on mercury electrodes. *Biophys. J.* 66:1969–1980.

Moncelli, M. R., L. Becucci, A. Nelson, and R. Guidelli. 1996. Electrochemical modeling of electron and proton transfer of ubiquinone-10 in a self-assembled phospholipid monolayer. *Biophys. J.* 70:2716–2726.

Moncelli, M. R., L. Becucci, F. Tadini Buoninsegni, and R. Guidelli. 1998b. Surface dipole potential at the interface between water and self-assembled monolayers of phosphatidylserine and phosphatidic acid. *Biophys. J.* 74:2388–2397.

Moncelli, M. R., R. Herrero, L. Becucci, and R. Guidelli. 1995. Adsorption of tetraphenylphosphonium and tetraphenylborate in self-assembled phosphatidylcholine and phosphatidylserine monolayers deposited on mercury electrodes. *J. Phys. Chem.* 99:9940–9951.

Moncelli, M. R., R. Herrero, L. Becucci, and R. Guidelli. 1998a. Kinetics of electron and proton transfer to ubiquinone-10 and from ubiquinol-10 in a self-assembled phosphatidylcholine monolayer. *Biochim. Biophys. Acta.* 1364:373–384.

Nelson, A. 1991. Electrochemical studies of thallium(I) transport across gramicidin modified electrode-adsorbed phospholipid monolayers. *J. Electroanal. Chem.* 303:221–236.

Nelson, A. 1992. Voltammetry of retinal in phospholipid monolayers adsorbed on mercury. *J. Electroanal. Chem.* 335:327–343.

Nelson, A. 1996. Influence of biologically active compounds on the monomolecular gramicidin channel function in phospholipid monolayers. *Langmuir.* 12:2058–2067.

Nelson, A. 1997. Influence of fixed charge and polyunsaturated compounds on the monomolecular gramicidin channel function in phospholipid monolayers: further studies. *Langmuir.* 13:5644–5651.

Nelson, A., and A. Benton. 1986. Phopholipid monolayers at the mercury/water interface. *J. Electroanal. Chem.* 202:253–270.

Nelson, A., and D. Bizzotto. 1999. Chronoamperometric study of Tl(I) reduction at gramicidin-modified phospholipid-coated mercury electrodes. *Langmuir.* 15:7031–7039.

Pohl, P., T. I. Rokitskaya, E. E. Pohl, and S. M. Saparov. 1997. Permeation of phloretin across bilayer lipid membranes monitored by dipole potential and microelectrode measurements. *Biochim. Biophys. Acta.* 1323: 163–172.

Providence, L. L., O. S. Andersen, D. V. Greathouse, R. E. Koeppe, II, and R. Bittman. 1995. Gramicidin channel function does not depend on phospholipid chirality. *Biochemistry.* 34:16404–16411.

Rokitskaya, T. I., Y. N. Antonenko, and E. A. Kotova. 1997. Effect of the dipole potential of a bilayer lipid membrane on gramicidin channel dissociation kinetics. *Biophys. J.* 73:850–854.

Rueda, M., I. Navarro, G. Ramirez, F. Prieto, C. Prado, and A. Nelson. 1999. Electrochemical impedance study of Tl^+ reduction through gramicidin channels in self-assembled gramicidin-modified dioleoylphosphatidylcholine monolayers on mercury electrodes. *Langmuir.* 15: 3672–3678.

Sandblom, J., G. Eisenman, and E. Neher. 1977. Ionic selectivity, saturation and block in gramicidin A channels. I. Theory for the electrical properties of ion selective channels having two pairs of binding sites and multiple conductance states. *J. Membr. Biol.* 31:383–417.

Seoh, S.-A., and D. Busath. 1995. Gramicidin tryptophans mediate formamidinium-induced channel stabilization. *Biophys. J.* 68:2271–2279.

Tredgold, R. H., and P. N. Hole. 1976. Dielectric behavior of dry synthetic polypeptides. *Biochim. Biophys. Acta.* 443:137–142.

Urban, B. W., S. B. Hladky, and D. A. Haydon. 1980. Ion movements in gramicidin pores. An example of single-file transport. *Biochim. Biophys. Acta.* 602:331–354.

Wallace, B. A. 1996. The role of tryptophan residues in the structure, function, and folding of the gramicidin transmembrane ion channel. *Adv. Exp. Med. Biol.* 398:607–614.